NEURAL NETWORK SHAPE: ORGAN SHAPE REPRESENTATION WITH RADIAL BASIS FUNCTION NEURAL NETWORKS

Guoyu Lu, Li Ren, Abhishek Kolagunda and Chandra Kambhamettu

Department of Computer and Information Science, University of Delaware, USA

ABSTRACT

We propose to represent the shape of an organ using a neural network classifier. The shape is represented by a function learned by a neural network. Radial Basis Function (RBF) is used as the activation function for each perceptron. The learned implicit function is a combination of radial basis functions, which can represent complex shapes. The organ shape representation is learned using classification methods. Our testing results show that the neural network shape provides the best representation accuracy. The use of RBF provides a rotation, translation and scaling invariant feature to represent the shape. Experiments show that our method can accurately represent the organ shape.

Index Terms— Shape Presentation, RBF Kernel, Artificial Neural Network, 3D Reconstruction

1. INTRODUCTION

Medical image analysis is an important tool to help diagnosis. To analyze an organ accurately, doctors usually capture 3D Magnetic Resonance (MR) images of the organ. For each MR image, the most observable and useful information is the organ boundary shown in the images. Manually segmenting the boundary of all the organ images is tedious and not objective. To relieve the manual work and improve the boundary detection, we propose to use vision and machine learning methods, to automatically detect organ boundary based on the learned organ shape. Through detected boundary, we can also compare the differences between various organ shapes.

Parametrized 2D to 3D surface reconstruction has been widely applied as morphable models [1, 2] where the 3D surface is automatically generated from multiple 2D photographs. The morphable models have been applied to more general shapes, such as cars and animals [3], as well as human bodies [4]. Partial differential equations [5, 6, 7] for solving signed distance functions and continuous functions from a set of disorganized point samples [8, 9] are also applied to estimate surfaces. Machine learning approaches are used to build local or global surface function based on a combination of radial basis functions (RBF) [10, 11] to describe the surface curves [12, 13, 11]. Current research transforms the contour points in 2D image to 3D shape in order to better study the shape properties. By applying kernel machine mapping similarity function from a point space to a Hilbert space, the surface of the 3D object can be represented as the hyperplane for classifying the point cloud data [14]. Gorelick et al. [15] assigned for every silhouette internal point a value which reflects the mean time required for a random walk beginning at this point to hit the boundaries. The boundary representation function is calculated by solving Poisson equation. The Support Vector Machine (SVM) with Radial Basis Function (RBF) kernel was further explored to represent sparse subset of points (support vector) by a set of radial basis functions [16]. Liu et al. [17] used the total Bregman Divergence (tBD) based l1-norm center as the representative of a set of shapes for the efficient and robust distance measure of dissimilarity between shapes of tBD.

Making use of the ground truth of the organ point cloud boundary, we create the positive boundary points and the negative boundary points by scaling up and down ground truth boundary points, which are later used for training the classifier. We use several different classification methods and compare the performance of different approaches. In our training phase, we train the boundary classification methods with three groups of points. The three labeled groups of points are points outside the boundary marked as -1, points on the boundary marked as 0 and points inside boundary marked as 1. Based on the trained classifiers, we can obtain a combination of radial basis functions with neural network representing an organ shape and detect the boundary points lying on the shape.

To summarize the contribution of our paper, we use Neural Network with radial basis function in perceptrons to represent shape. The combination of learned RBF functions can accurately describe the shape mathematically. Meanwhile, different from support vector shape [16], the use of Neural Network can represent the shape with 3 classes of points, making the shape representation more accurate.

2. 3D POINTS CLASSIFICATION

As our purpose is to represent organ shape based on classification method, we test several classic classification methods (Naive Bayes, Neural Network, nearest neighbour and SVM-RBF kernel) on the effect of separating points on the shape boundary out of all other points not on the boundary. The test is conducted on a public liver dataset [18]. The training points are separated into 3 groups, points outside of the boundary, points on the boundary and points inside the boundary. The three classes are labeled -1, 0 and 1 separately. In testing, the points outside and inside the boundary are treated as the negative examples. Points on the boundary are considered as the positive samples. The boundary points are determined by the probability that the point is classified into outside, boundary and inside points groups. The points with the highest probability for the boundary class are considered lying on the surface. The classification accuracy result is shown in Table 1.

Method	Mean	variance	round 1	round 2	round 3	round 4	round 5
Naive Bayes	0.4329	0.0027	38.63%	48.19%	49.59%	40.23%	39.80%
Neural Network	0.7872	0.0256	75.59%	93.98%	92.23%	77.49%	54.32%
Nearest Neighbor	0.3437	2.02E-4	32.39%	35.02%	36.09%	33.58%	34.79%
5 Nearest Neighbor	0.2607	1.82E-4	23.83%	26.41%	27.48%	26.19%	26.44%
RBF Kernel	0.3302	4.17E-4	50.21%	54.81%	60.15%	52.01%	42.91%

Table 1: The liver prediction accuracy based on different methods on 3 classes.

From Table 1, we can observe that after dividing the training data into 3 classes, Neural Network can significantly outperform all other classification methods. It shows us when dealing with multi-class classification problems, Neural Network can outperform most other classification algorithms, especially when the data is not linearly separable. For this reason, we select Neural Network to further represent organ shapes.

Since we have the ground truth boundary points, we manually create non-boundary points for the classification purpose. All the reconstructed points on the boundary are scaled up as the outside boundary class. Inside boundary points are generated similarly by scaling down. The outside, inside and the ground truth points (boundary) are shown in Fig.1, from which we can see that the three groups of points wrap each other well, implying they are easily separable.

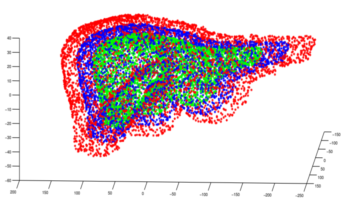

Fig. 1: 3D point cloud for inside points (green), ground truth points (blue) and outside points (red).

3. NEURAL NETWORK RBF SHAPE REPRESENTATION

In Neural Networks (ANN), the perceptron is the basic processing element which receives input from the neural network environment and outputs to other perceptrons. For N inputs and M outputs, the RBF network can be expressed as:

$$\begin{aligned} &y = f(u), f : R^N -> R^M \\ &y_j = f_j(u) = w_{0j} + \sum_{i=1}^{L} w_{ij} G(\|u - c_i\|) j = 1, ..., M \end{aligned} \quad (1)$$

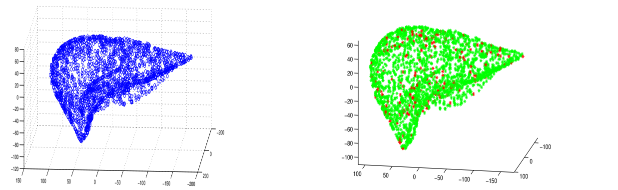

(a) The ground truth of liver boundary.

(b) The estimated liver boundary shape based on RBF-Neural Network.

Fig. 2: The ground truth and the estimated boundary shape. In Fig.2(b), green points are the points correctly appeared in the estimated boundary. Red points represent points which are ground truth points, but do not appear in the estimated boundary.

where u is the input vector and c_i is the center of Gaussian or Multivariate Gaussian basis function. y_j is the label for the j th element. The normalization form is represented as the following equation:

$$y = f(u) = \frac{\sum_{i=1}^{N} w_i G(\|u - c_i\|)}{\sum_{i=1}^{N} G(\|u - c_i\|)} \quad (2)$$

The training step can be divided into two steps: first we need to generate the centers of basis function from samples, then optimize the weights of hidden output. For the first step, we use k-means clustering to estimate the centers of basis function. Given input training patterns $\{u^k, y^k\}$, the second step is to minimize the following objective function by choosing optimized weights w.

$$J(w, c) = \sum_{k=1}^{K} \left\| y^k - f(u^k) \right\|^2 \quad (3)$$

In each step, the weights are modified by moving them in the direction opposite to the gradient of the objective function.

$$w(k+1) = w(k) - v \frac{\partial J_k(w, c)}{\partial w} \quad (4)$$

v is the learning rate. In this case, the training linear weights w_i becomes:

$$w_i(k+1) = w_i(k) + v(y^k - f(u^k)) G(\left\| u^k - c_i \right\|) \quad (5)$$

The whole process is combined with back propagation to optimize the learning process. After learning, each RBF perceptron is associated with a weight. The combination of weighted RBF perceptions can accurately represent shape.

4. EXPERIMENTS RESULT

4.1. Experiments on Liver Dataset

We test our method on public liver dataset [18]. Due to the data availability limitation, we use 5-fold cross validation—$3/5$ of the points are randomly picked for training and the rest

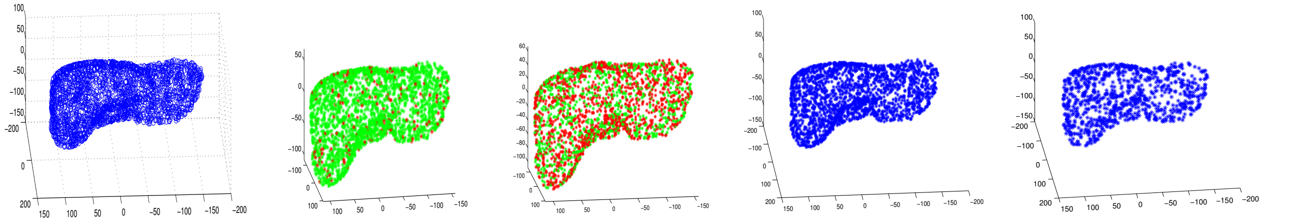

(a) (b) (c) (d) (e)

Fig. 3: Our RBF liver comparison result: (a) The liver ground truth shape. (b) The liver boundary points classification result by RBF-Neural Network. Red represents wrong classification points. Green are the correct classified points. (c) The liver boundary points classification result by SVM-RBF [16]. (d) The liver shape estimated by RBF-Neural Network. (e) The liver shape estimated by SVM-RBF [16].

$2/5$ of the data serves for the testing purpose. The estimated boundary shape and the ground truth are presented in Fig.2.

From Fig.2, we can observe that almost all the ground truth points are also shown on the Neural Network estimated boundary, with few points missing in the estimated boundary. The boundary estimated by RBF-Neural Network can accurately describe the shape of the liver in a 3D environment. The comparison between SVM-RBF [16] and RBF-Neural Network is shown in Fig.6(b) and Fig.6(c).

Fig.6(b) and Fig.6(c) show that many boundary points are incorrectly classified in SVM-RBF compared with RBF-Neural Network. The points are almost all correctly classified by RBF-Neural Network. The learned shape is implicitly represented as the zero level set of the sum of weighted RBFs. The shape comparison can be achieved by computing the RBF parameters. To visualize the represented shape, we uniformly generate points in a 3D space of $1000*1000*1000$, $[-49, 50]$ for each dimension. The points are generated in every 0.1 step. We extract points that fit the learned shape representation (meaning the points are on the boundary) and visualize them. From Fig. 6(e) and Fig.6(d), we observe that the liver boundary estimated by RBF-Neural Network is much closer to the ground truth compared to SVM-RBF. Meanwhile, the RBF-Neural Network estimated boundary contains much more points compared with SVM-RBF boundary, indicating that more boundary points are obtained correctly. Our method can accurately represent the liver shape. Using the points that fit the learned representation, we build the dense liver surface by Poisson reconstruction, as shown in Fig.4(a). The surface of the liver is smooth based on the shape represented by RBF-Neural Network in a more compact way rather than original point cloud. The Poisson reconstruction model is used for quantitatively measuring the accuracy of the 3D shape estimation. We register the estimated 3D shape to the ground truth Poisson reconstruction model through iterative closest point (ICP) [19] and record the distance of each point on the estimated shape. The smaller distance, the more accurate model estimated. We compare our RBF-Neural Network method with the other state-of-the-art approaches (Poisson Shape [15], Total Bregman Divergence Shape [17] and SVM-RBF [16]) with average point distance error through the whole dataset, shown in Fig.4(b).

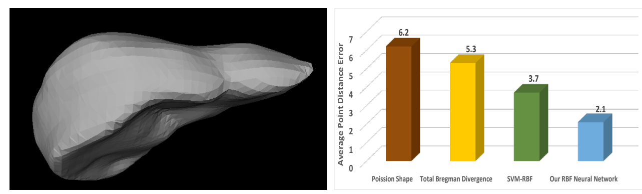

(a) (b)

Fig. 4: (a) Shape of our RBF-neural network liver after Poisson reconstruction. (b) RBF-Neural Network average point distance error compared with Poisson shape [15], Total Bregman Divergence shape [17] and SVM-RBF shape [16].

From Fig.4(b), our method can reduce 43.2%, 60.4% and 66.1% shape estimation error respectively based on SVM-RBF shape (SVS) [16], Total Bregman Divergence method [17] and Poisson shape [15], proving our method applicable for shape representation task. More liver shape representation result samples are provided in Fig. 6.

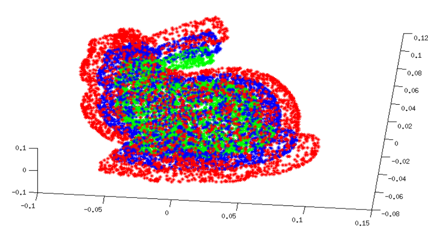

Fig. 5: 3D point cloud for inside points (green), ground truth points (blue) and outside points (red) for bunny model.

4.2. Experiments on Non-medical Shape Representation

We also conduct our experiments on Stanford bunny dataset [20, 21] for testing our method's effect on non-medical shape representation. We still train our shape model through training classification model that distinguishes the points outside the model, lying on the model and inside the model (Fig.5). We further compare our RBF-Neural Network model shape representation together with the SVM-RBF shape (Fig.7). From Fig.7 , we can observe that our RBF-Neural Network model significantly outperform SVM-RGB model on representing the bunny model shape in terms of accuracy. When

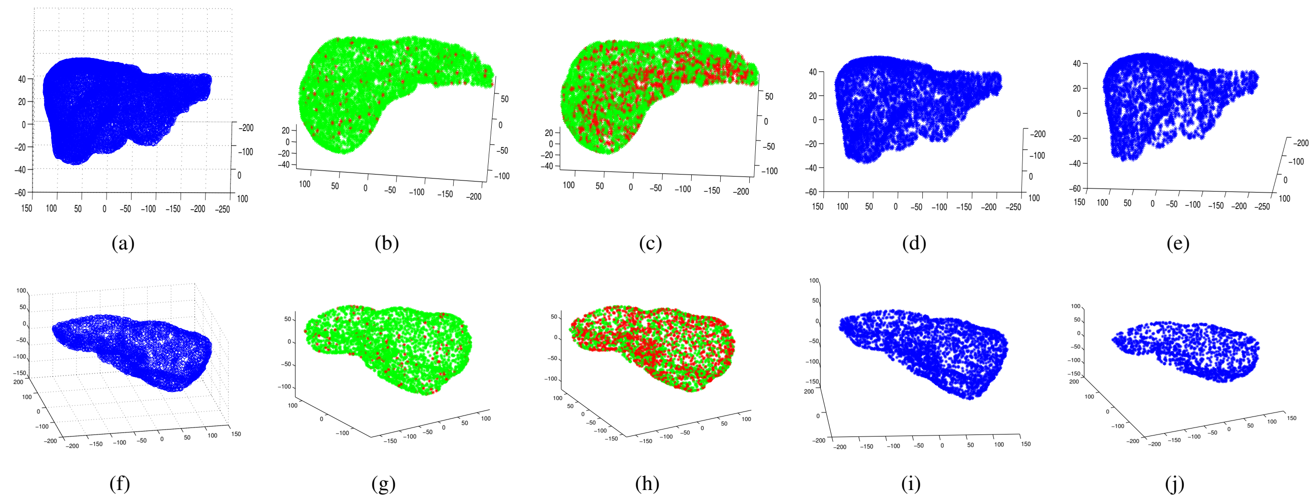

Fig. 6: RBF liver comparison result from different views: (a, f) The liver ground truth shape. (b, g) The liver boundary points classification result by RBF-Neural Network. (c, h) The liver boundary points classification result by SVM-RBF [16]. (d, i) The liver shape estimated by RBF-Neural Network. (e, j) The liver shape estimated by SVM-RBF [16].

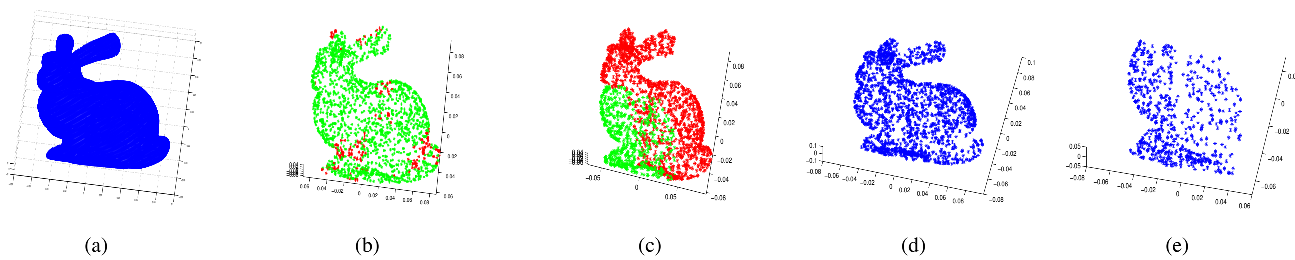

Fig. 7: Our RBF bunny comparison result: (a) The bunny ground truth shape. (b) The bunny boundary points classification result by RBF-Neural Network. Red represents wrong classification points. Green are the correct classified points. (c) The bunny boundary points classification result by SVM-RBF [16]. (d) The bunny shape estimated by RBF-Neural Network. (e) The bunny shape estimated by SVM-RBF [16].

the model shape becomes more complex, the advantage is even more obvious. Fig.7 also shows that our shape representation method is not only suitable for organ shape representation, but also ideal for representing any other complex model shape.

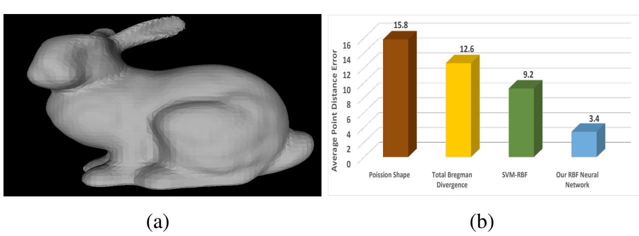

Fig. 8: (a) Poisson reconstruction model based on our RBF-Neural Network for bunny. (b) Our RBF-Neural Network average point distance error compared with Poisson shape [15], Total Bregman Divergence shape [17] and SVM-RBF shape [16] on bunny model.

We also conduct experiments similar to Fig.4(b) on bunny dataset. The calculated error distance is shown in Fig.8(b), from which we can notice that when the model becomes more complex, the advantage of our method is getting more obvious, resulting in much smaller error than other methods. The Poisson reconstruction model of the bunny is shown in Fig.8(a). We can see that even with complex changes, the final representation shape is still accurate and smooth.

5. CONCLUSION

We make use of point cloud to learn neural network shape. We test different classification methods on the task of organ boundary prediction. Using the ground truth of the boundary points, we create scaled boundaries for training classifiers. We treat the points outside, inside and on the boundary as 3 different classes for training the classifiers. Testing results show that RBF-Neural Network dramatically outperforms other methods of classification. We make use of the radial basis functions in the perceptrons and learn the final shape representation as a combination of radial basis functions. Gradient descent and back propagation methods are applied to update the weight of each perceptron. Experimental results show that our method can not only accurately represent shapes of different organs, but also represent other complex shapes in a high accuracy.

6. REFERENCES

[1] J. M. Reinhardt and W. E. Higgins, "Toward efficient morphological shape representation," in *International Conference on Acoustics, Speech and Signal Processing (ICASSP)*, 1993, pp. 125–128.

[2] V. Blanz and T. Vetter, "A morphable model for the synthesis of 3d faces," in *The Annual Conference on Computer Graphics (SIGGRAPH)*, 1999.

[3] C. R. Shelton, "Morphable surface models," *International Journal on Computer Vision*, vol. 38, no. 1, 2000.

[4] B. Allen, B. Curless, and Z. Popović, "The space of human body shapes: reconstruction and parameterization from range scans," *ACM Transactions on Graphics*, vol. 22, no. 3, 2003.

[5] K. Museth, D. E. Breen, R. T. Whitaker, and A. H. Barr, "Level set surface editing operators," in *ACM Transactions on Graphics*, vol. 21, no. 3, 2002.

[6] T. Kim, J. Tessendorf, and N. Thuerey, "Closest point turbulence for liquid surfaces," *ACM Transactions on Graphics*, vol. 32, no. 2, 2013.

[7] L. G. Zagorchev and A. A. Goshtasby, "A curvature-adaptive implicit surface reconstruction for irregularly spaced points," *IEEE Transactions on Visualization and Computer Graphics*, vol. 18, no. 9, 2012.

[8] A. A. Taflanidis and S.-H. Cheung, "Stochastic sampling using moving least squares response surface approximations," *Probabilistic Engineering Mechanics*, vol. 28, 2012.

[9] P. Breitkopf, H. Naceur, A. Rassineux, and P. Villon, "Moving least squares response surface approximation: Formulation and metal forming applications," *Computers & Structures*, vol. 83, no. 17, 2005.

[10] J. C. Carr, R. K. Beatson, J. B. Cherrie, T. J. Mitchell, W. R. Fright, B. C. McCallum, and T. R. Evans, "Reconstruction and representation of 3d objects with radial basis functions," in *The Annual Conference on Computer Graphics (SIGGRAPH)*, 2001.

[11] B. S. Morse, T. S. Yoo, P. Rheingans, D. T. Chen, and K. R. Subramanian, "Interpolating implicit surfaces from scattered surface data using compactly supported radial basis functions," in *The Annual Conference on Computer Graphics (SIGGRAPH)*, 2005.

[12] J. Ben-Arie, Z. Wang, and K. R. Rao, "Affine invariant shape representation and recognition using gaussian kernels and multi-dimensional indexing," in *International Conference on Acoustics, Speech and Signal Processing (ICASSP)*, vol. 6, 1996, pp. 3470–3473.

[13] C. J. Walder and B. C. Lovell, "Kernel based algebraic curve fitting," in *International Conference on Advances in Pattern Recognition (ICAPR)*, vol. 1, 2003.

[14] F. Steinke, B. Schölkopf, and V. Blanz, "Support vector machines for 3d shape processing," in *Computer Graphics Forum*, vol. 24, no. 3, 2005.

[15] L. Gorelick, M. Galun, E. Sharon, R. Basri, and A. Brandt, "Shape representation and classification using the poisson equation," *IEEE Transactions on Pattern Analysis and Machine Intelligence*, vol. 28, no. 12, 2006.

[16] H. Van Nguyen and F. Porikli, "Support vector shape: A classifier-based shape representation," *IEEE Transactions on Pattern Analysis and Machine Intelligence*, vol. 35, no. 4, 2013.

[17] M. Liu, B. C. Vemuri, S.-I. Amari, and F. Nielsen, "Shape retrieval using hierarchical total bregman soft clustering," *IEEE Transactions on Pattern Analysis and Machine Intelligence*, vol. 34, no. 12, 2012.

[18] T. Heimann et al., "Comparison and evaluation of methods for liver segmentation from ct datasets," *IEEE Transactions on Medical Imaging*, vol. 28, no. 8, pp. 1251–1265, 2009.

[19] P. J. Besl and N. D. McKay, "Method for registration of 3-d shapes," in *Robotics-DL tentative*, 1992.

[20] G. Turk and M. Levoy, "Zippered polygon meshes from range images," in *The Annual Conference on Computer Graphics and Interactive Techniques*, 1994, pp. 311–318.

[21] A. Gardner, C. Tchou, T. Hawkins, and P. Debevec, "Linear light source reflectometry," in *ACM Transactions on Graphics*, vol. 22, no. 3, 2003, pp. 749–758.